A Simple, Efficient Synthetic Route to $Sr_2Si_5N_8$:Eu^{2+}-Based Red Phosphors for White Light-Emitting Diodes

Rong-Jun Xie,*,† Naoto Hirosaki,† Takayuki Suehiro,‡ Fang-Fang Xu,§ and Mamoru Mitomo†

Nano Ceramics Center, National Institute for Materials Science, Namiki 1-1, Tsukuba, Ibaraki 305-0044, Japan Institute of Multidisciplinary Research and Advanced Materials, Tohoku University, Katahira 2-1-1, Aoba-ku, Sendai, 980-8577, Japan Shanghai Institute of Ceramics, Chinese Academy of Science, 1295 Dingxi Road, Shanghai 20050, China

Received May 2, 2006. Revised Manuscript Received September 12, 2006

This paper reports a simple, inexpensive, and high-yield synthetic route to $Sr_2Si_5N_8$:Eu^{2+}-based red nitridosilicate phosphors for white light-emitting diodes (LEDs). Through the chemical reaction of $SrCO_3$, Eu_2O_3, and Si_3N_4 rather than the air-sensitive Sr, Eu, $Si(NH)_2$, Sr_3N_2, and EuN powders, a complex phosphor consisting of $Sr_2Si_5N_8$:Eu^{2+} (∼64 wt %) and Sr_2SiO_4:Eu^{2+} (∼36 wt %) were obtained by firing the powder mixture at 1600 °C under 0.5 MPa N_2. The structural characterization, luminescence spectra, quantum efficiency, and thermal quenching of the synthesized phosphor were investigated and compared with those of $Sr_2Si_5N_8$:Eu^{2+} prepared by the conventional method. It shows that the emission of the existing Sr_2SiO_4:Eu^{2+} is extremely low (about 0.04% of that of $Sr_2Si_5N_8$:Eu^{2+}) under the ultraviolet-light irradiation, and it is silent under the blue-light excitation ($\lambda = 400-480$ nm); therefore, the luminescence of the complex phosphor solely arises from $Sr_2Si_5N_8$:Eu^{2+}. The $Sr_2Si_5N_8$:Eu^{2+}-based phosphor is orange-red in color and emits strongly in the red region of 616−670 nm depending on the Eu^{2+} concentration when excited at $\lambda = 450$ nm. Furthermore, the $Sr_2Si_5N_8$:Eu^{2+}-based phosphor synthesized by this novel method shows equivalent optical properties, such as high emission intensity, high quantum efficiency, and very low thermal quenching, with those prepared by the conventional approaches, allowing it a promising red luminescent material for white LEDs.

1. Introduction

Nitridosilicates, oxonitridosilicates, or oxonitridoaluminosilicates, which are derived from oxosilicates by formal exchanges of oxygen by nitrogen and/or silicon by aluminum, are of great interest owing to their outstanding thermal, chemical, and mechanical stability and structural diversity.[1,2] Very recently, these compounds have been extensively studied as host lattices for phosphors, which exhibit unusual, interesting luminescence properties when activated by rare-earth ions, such as $Ba_2Si_5N_8$:Eu^{2+},[3] α-SiAlON:RE (RE = Eu^{2+}, Ce^{3+}, Yb^{2+}, Tb^{3+}, Pr^{3+}, Sm^{3+}),[4−9] β-SiAlON:Eu^{2+},[10] $M_2Si_5N_8$:Eu^{2+},Ce^{3+},[11,12] $MSi_2O_{2-\delta}N_{2+2/3\delta}$:$Eu^{2+}$,$Ce^{3+}$,[13,14] and $CaAlSiN_3$:Eu^{2+}.[15] Most importantly, these phosphors emit visible light efficiently under near-ultraviolet or blue light irradiation and have superior thermal and chemical stability to their oxide and sulfide counterparts, allowing them to be used as down-conversion luminescent materials for white light-emitting diodes (LEDs).[5−15] Nitridosilicate $Sr_2Si_5N_8$:Eu^{2+} shows orange-red emission and has high quantum efficiency and very low thermal quenching, which makes it an encouraging red phosphor for use in white light-emitting diodes to improve the color rendering index.[16]

Two common synthetic strategies for $Sr_2Si_5N_8$:Eu^{2+} have been proposed in the literature. The first one involves the reaction of stoichimetric amounts of strontium metal (Sr) and europium metal (Eu) with silicon diimide ($Si(NH)_2$) in a radio frequency furnace (route 1):[17]

$$(2-x)\mathrm{Sr} + x\mathrm{Eu} + 5\mathrm{Si(NH)_2} \rightarrow \mathrm{Sr_{2-x}Eu_xSi_5N_8} + \mathrm{N_2} + 5\mathrm{H_2} \quad (1)$$

The second one involves the reaction of strontium nitride

* Corresponding author. Tel.: +81-29-860-4312. Fax: +81-29-851-3613. E-mail: Xie.Rong-Jun@nims.go.jp.
† National Institute for Materials Science.
‡ Tohoku University.
§ Chinese Academy of Science.

(1) Schnick, W. *Int. J. Inorg. Mater.* **2001**, *3*, 1267.
(2) Schnick, W.; Huppertz, H. *Chem. Eur. J.* **1997**, *3*, 679.
(3) Hoppe, H. A.; Lutz, H.; Morys, P.; Schnick, W.; Seilmeier, A. *J. Phys. Chem. Solids* **2000**, *61*, 2001.
(4) Xie, R.-J.; Mitomo, M.; Uheda, K.; Xu, F.-F.; Akimune, Y. *J. Am. Ceram. Soc.* **2002**, *85*, 1229.
(5) Xie, R.-J.; Hirosaki, N.; Mitomo, M.; Yamamoto, Y.; Suehiro, T.; Sakuma, K. *J. Phys. Chem. B* **2004**, *108*, 12027.
(6) Xie, R.-J.; Hirosaki, N.; Sakuma, K.; Yamamoto, Y.; Mitomo, M. *Appl. Phys. Lett.* **2004**, *84*, 5404.
(7) Xie, R.-J.; Hirosaki, N.; Mitomo, M.; Uheda, K.; Suehiro, T.; Xu, X.; Yamamoto, Y.; Sekiguchi, T. *J. Phys. Chem. B* **2005**, *109*, 9490.
(8) Xie, R.-J.; Hirosaki, N.; Mitomo, M.; Takahashi, K.; Sakuma, K. *Appl. Phys. Lett.* **2006**, *88*, 101104.
(9) van Krevel, J. W. H.; van Rutten, J. W. T.; Mandal, H.; Hintzen, H. T.; Metselaar, R. *J. Solid State Chem.* **2002**, *165*, 19.
(10) Hirosaki, N.; Xie, R.-J.; Kimoto, K.; Sekiguchi, T.; Yamamoto, Y.; Suehiro, T.; Mitomo, M. *Appl. Phys. Lett.* **2005**, *86*, 211905.
(11) van Krevel, J. W. H. Ph.D. Thesis, Eindhoven University of Technology, 2000.
(12) Li, Y. Q.; de With, G.; Hintzen, H. T. *J. Lumin.* **2006**, *116*, 107.
(13) Li, Y. Q.; de With, G.; Hintzen, H. T. *J. Mater. Chem.* **2005**, *15*, 4492.
(14) Li, Y. Q.; Delsing, A. C. A.; de With, G.; Hintzen, H. T. *Chem. Mater.* **2005**, *15*, 4492.
(15) Uheda, K.; Hirosaki, N.; Yamamoto, Y.; Naoto, A.; Nakajima, T.; Yamamoto, H. *Electrochem. Solid State Lett.* **2006**, *9*, H22.

10.1021/cm061010n CCC: $33.50
Published on Web 10/19/2006

(Sr_3N_2) and europium nitride (EuN) with silicon nitride (Si_3N_4) in a horizontal tube or graphite furnace (route 2) under a nitrogen atmosphere:[11,12]

$$(2-x)Sr_3N_2 + 3xEuN + 5Si_3N_4 \rightarrow 3Sr_{2-x}Eu_xSi_5N_8 + 0.5xN_2 \quad (2)$$

The raw powders such as $Si(NH)_2$ and EuN are not only expensive but also not commercially available, and they have to be synthesized at the laboratory first. Furthermore, the powder mixing must be handled in a dry, nitrogen-filled glove box because the raw materials are very sensitive to oxygen and moisture. Thus, both of the above-mentioned synthetic methods are associated with multistep and complex procedures, difficulty in handling, high costs, and low yields. Recently, the carbothermal reduction and nitridation (CRN) method has been used to produce $Sr_2Si_5N_8$:Eu^{2+} based on the following chemical reaction (route 3):[18]

$$SrO + Si_3N_4 + Eu_2O_3 + C + N_2 \rightarrow (Sr_{1-x}Eu_x)_2Si_5N_8 + CO \quad (3)$$

This method will, with no doubts, introduce residual carbon into the phosphor, which reduces its absorption and emission significantly. To remove the residual carbon, annealing the powder in air or oxygen at temperatures above 600 °C is required. However, Krevel et al.[11] has reported that no red emission is observed for $Sr_2Si_5N_8$:Eu^{2+} after a heat treatment at 600 °C for 2 h, due to the oxidation of Eu^{2+} to Eu^{3+}. It implies that complete removal of the residual carbon in the synthesized powder still remains unresolved. Therefore, developing an inexpensive, straightforward, and efficient method to synthesize a high-brightness $Sr_2Si_5N_8$:Eu^{2+} red phosphor is in great demand from the viewpoint of industrial applications and remains an important task for materials scientists.

Here, we report a novel synthetic route to $Sr_2Si_5N_8$:Eu^{2+}-based red nitridosilicate phosphors based on a direct reaction among strontium carbonate ($SrCO_3$), Eu_2O_3, and Si_3N_4 (route 4). All the raw materials used are commercially available and relatively inexpensive, and the handling of raw powders can be done in an ambient atmosphere, which therefore makes it a simple, efficient, and high-yield route to $Si_2Si_5N_8$:Eu^{2+}. The structure and the luminescence properties of the synthesized $Si_2Si_5N_8$:Eu^{2+}-based phosphor were investigated and compared with those of the phosphor prepared by route 2. We have shown that $Si_2Si_5N_8$:Eu^{2+} synthesized by this method has comparable optical properties with those of the phosphors prepared by the traditional approaches, and these phosphors are suitable for use as a red phosphor for white LEDs.

2. Experimental Section

2.1. Preparation of $Sr_2Si_5N_8$:Eu^{2+}. $Sr_2Si_5N_8$:Eu^{2+}-based red phosphors were prepared by a solid-state reaction of $SrCO_3$ (Eu_2O_3) and Si_3N_4 with the ratio of 2:1. α-Si_3N_4 (SN-E10, Ube Industries, Tokyo, Japan), Eu_2O_3 (Shin-Etsu Chemical Co. Ltd., Tokyo, Japan), and $SrCO_3$ (Sigma-Aldrich Japan K.K., Tokyo, Japan) were used as starting powders and mixed in ethanol for 2 h. The concentration of Eu^{2+} varied in a range of 0−20 mol % with respect to Sr^{2+}. After drying, the powder mixture was fired at 1600 °C for 2 h under a 0.5 MPa N_2 using a gas-pressure sintering furnace (FVPHR-R-10, FRET-40, Fujidempa Kogyo Co. Ltd., Osaka, Japan) with a graphite heater. For comparison, $Sr_2Si_5N_8$:Eu^{2+} was also prepared by route 2, i.e., by firing the powder mixture of α-Si_3N_4 (SN-E10, Ube Industries, Tokyo, Japan), Sr_3N_2 (Kojundo Chemical Laboratory Co. Ltd., Tokyo, Japan), and EuN according to route 2 at 1600 °C for 12 h under 0.5 MPa N_2. EuN was synthesized by the reaction of metallic Eu with N_2 at 850 °C for 6 h in a tube furnace. The powder mixture was conducted under a continuously purified nitrogen atmosphere in a glove box (MBRAUN Unilab, MBRAUN GmbH, Germany). The concentration of oxygen and moisture is <1 ppm, respectively.

2.2. Structural Characterization. The X-ray diffraction pattern of the as-synthesized powder was recorded with a Rigaku RINT2000 system using Cu $K\alpha_1$ ($\lambda = 1.5408$ Å). Data were collected over the 2θ range of 10−130°, with a step width of 0.02° and count time of 12 s/step. The multiphase Rietveld analysis was conducted using the program RIETAN-2000.[19] The particle morphology of the as-synthesized powder was observed by a scanning electron microscope (S-5000, Hitachi Ltd., Tokyo, Japan). Electron diffraction patterns and TEM micrographs were obtained on a field-emission transmission electron microscope (JEM-2100F, JEOL Ltd., Tokyo, Japan).

2.3. Luminescence Properties Measurement. The photoluminescence spectra were measured at room temperature using a fluorescent spectrophotometer (F-4500, Hitachi Ltd., Tokyo, Japan) with a 200 W Xe lamp as an excitation source. The emission spectrum was corrected for the spectral response of a monochromator and Hamamatsu R928P photomultiplier tube by a light diffuser and tungsten lamp (Noma, 10V, 4A). The excitation spectrum was also corrected for the spectral distribution of the xenon lamp intensity by measuring Rhodamine-B as reference. The temperature-dependent luminescence (25−200 °C) was conducted with a 200 W Xe lamp as an excitation source and a Hamamatsu MPCD-7000 multichannel photodetector.

3. Results and Discussion

The undoped powder for structural analysis was obtained by heating the powder mixture of Si_3N_4 and $SrCO_3$ with the mole ratio of 1:2 at 1600 °C for 2 h under 0.5 MPa N_2. As shown in Figure 1, the synthesized powder by route 4 is a complex mixture, which consists of two types of particles: one is well-dispersed, uniform primary particles with a mean diameter of 0.5−0.8 μm (particle A) and the other is large, round-shaped particles with a mean diameter of 2.0−3.0 μm (particle B).

The X-ray diffraction pattern of the powder reveals three major phases of $Sr_2Si_5N_8$, α-Sr_2SiO_4, and β-Sr_2SiO_4, as shown in Figure 2. Structural refinement was further carried out by the Rietveld method, using the RIETAN-2000 program.[19] The published structural parameters of $Sr_2Si_5N_8$,[17] α-Sr_2SiO_4,[20] and β-Sr_2SiO_4[21] were used as the initial parameters for structural refinement of the prepared powder.

(16) Mueller-Mach, R.; Mueller, G.; Krames, M. R.; Hoppe, H. A.; Stadker, F.; Schinick, W.; Juestel, T.; Schmidt, P. *Phys. Status Solidi A* **2005**, *202*, 1727.
(17) Schlieper, T.; Milius, W.; Schnick, W. *Z. Anorg. Allg. Chem.* **1995**, *621*, 1380.
(18) Piao, X.; Horikawa, T.; Hanzawa, H.; Machida, K. *Appl. Phys. Lett.* **2006**, *88*, 161908.
(19) Izumi, F.; Ikeda, T. *Mater. Sci. Forum* **2003**, *198*, 321.
(20) Catti, M.; Gazzoni, G.; Ivaldi, G.; Zanini, G. *Acta. Crystallogr., Sect. B* **1983**, *39*, 674.

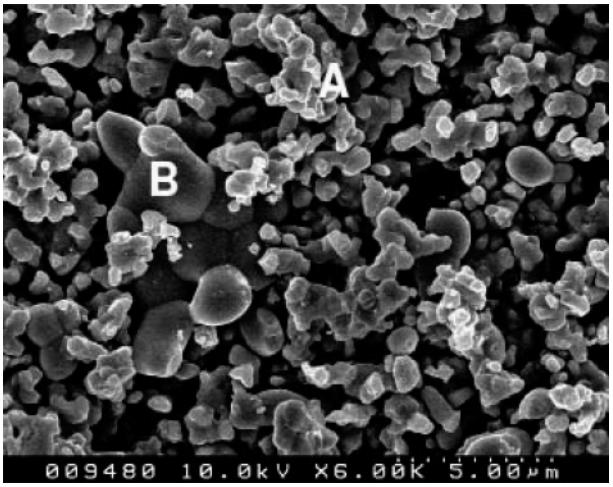

Figure 1. Scanning electron microscopy image of the as-synthesized powder by route 4.

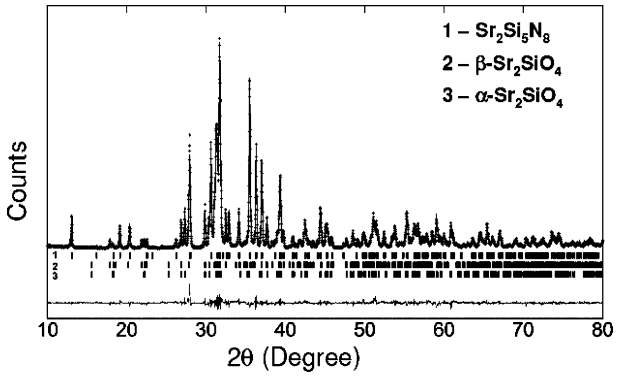

Figure 2. Rietveld refinement of the powder data of the as-synthesized powder by route 4.

Table 1. Atomic Coordinates, Site Occupancy Fraction (S.O.F.), and Isotropic Displacement Parameters of the First Phase $Sr_2Si_5N_8$ Refined from the X-ray Data[a]

atoms	site	S.O.F.	*x*/*a*	*y*/*b*	*z*/*c*	*B* (Å^2)
Sr1	2a	0.907(12)	0	0.8695	0	1.28
Sr2	2a	0.889(11)	0	0.8816	0.3686	1.33
Si1	4b	1.0	0.2518	0.6669	0.6836	0.81
Si2	2a	1.0	0	0.0549	0.6771	0.85
Si3	2a	1.0	0	0.4196	0.4619	0.89
Si4	2a	1.0	0	0.4014	0.9023	0.88
N1	2a	1.0	0	0.191	0.520	1.11
N2	4b	1.0	0.2478	0.9122	0.6728	1.46
N3	4b	1.0	0.2488	0.4443	0.0105	1.21
N4	2a	1.0	0	0.5871	0.7735	1.01
N5	2a	1.0	0	0.171	0.835	1.18
N6	2a	1.0	0	0.4270	0.2722	1.03

[a] Crystal structure: orthorhombic; space group: $Pmn2_1$ (No. 31); a = 5.7101(2) Å, b = 6.8213(2) Å, c = 9.3321(3) Å, R_B = 2.35%, R_F = 1.55%.

The experimental and calculated patterns are shown in Figure 2. The final reliability factors for the whole pattern are R_p = 8.24%, R_{wp} = 11.07%, and S = 1.25. Tables 1, 2 and 3 list the lattice constants, atomic coordinates, site occupancy fraction, and isotropic displacement parameters for respectively $Sr_2Si_5N_8$, β-Sr_2SiO_4, and α-Sr_2SiO_4. Refinement of the site occupancy of Sr significantly improved the reliability of pattern fitting, leading to slight deviation of the site occupancy fraction (S.O.F.) of Sr from unit. The S.O.F. of

(21) Catti, M.; Gazzoni, G.; Ivaldi, G. *Acta. Crystallogr., Sect. C* **1983**, *39*, 29.

Table 2. Atomic Coordinates, Site Occupancy Fraction (S.O.F.), and Isotropic Displacement Parameters of the Second Phase β-Sr_2SiO_4 Refined from the X-ray Data[a]

atoms	site	S.O.F.	*x*/*a*	*y*/*b*	*z*/*c*	*B* (Å^2)
Sr1	4e	1.0	0.2618	0.3425	0.5778	0.69
Sr2	4e	1.0	0.2698	0.0007	0.3023	0.28
Si	4e	1.0	0.2427	0.7781	0.5813	1.3
O1	4e	1.0	0.280	1.008	0.571	2.5
O2	4e	1.0	0.191	0.679	0.431	1.7
O3	4e	1.0	0.488	0.679	0.642	4.7
O4	4e	1.0	0.023	0.726	0.675	3.2

[a] Crystal structure: monoclinic; space group: $P1_{21}/n_1$ (No. 14); a = 5.6610(3) Å, b = 7.0838(4) Å, c = 9.7573(5) Å, β = 92.586(4)°, R_B = 2.51%, R_F = 1.62%.

Table 3. Atomic Coordinates, Site Occupancy Fraction (S.O.F.), and Isotropic Displacement Parameters of the Third Phase α-Sr_2SiO_4 Refined from the X-ray Data[a]

atoms	site	S.O.F.	*x*/*a*	*y*/*b*	*z*/*c*	*B* (Å^2)
Sr1	8d	1.0	0.3403	0.25	0.57938	0.77
Sr2	8d	1.0	−0.0013	0.25	0.30213	0.54
Si	4c	1.0	0.7786	0.25	0.5831	0.25
O1	8d	1.0	1.005	0.25	0.5683	2.8
O2	8d	1.0	0.676	0.25	0.4333	3.6
O3	8d	1.0	0.706	0.480	0.6639	2.5

[a] Crystal structure: orthorhombic; space group: *Pmnb* (No. 62); a = 7.0803(4) Å, b = 5.6709(3) Å, c = 9.7427(5) Å, R_B = 2.39%, R_F = 1.52%.

Sr1 and Sr2 is respectively 0.907(12) and 0.889(11), indicating slight deficiency of Sr at both sites. Therefore, the composition of the obtained $Sr_2Si_5N_8$ using route 4 can be estimated as $Sr_{1.8}Si_5O_{0.4}N_{7.6}$, taking the charge compensation into account. The refined lattice parameters of the as-synthesized $Sr_2Si_5N_8$ are a = 5.7101(2), b = 6.8213(2), and c = 9.3321(3) Å, which agree well with those prepared by route 1 (a = 5.710, b = 6.822, and c = 9.341 Å).[17] No appreciable changes of lattice parameters from the reported data for both silicates are observed. The quantitative analysis of $Sr_2Si_5N_8$, α-Sr_2SiO_4, and β-Sr_2SiO_4 in the powder prepared by route 4 is roughly made by the Rietveld refinement without considering the Brindley correction.[22] The estimated values of $Sr_2Si_5N_8$, α-Sr_2SiO_4, and β-Sr_2SiO in the complex mixture are about 64, 16, and 20 wt %, respectively.

The three phases were also analyzed by transmission electron microscopy (TEM), and the results are shown in Figure 3. The $Sr_2Si_5N_8$ phase shows fine crystallite particles with facets (corresponding to particle A in Figure 1), whereas the α-Sr_2SiO_4 and β-Sr_2SiO_4 phases exhibit large grains with round shape (corresponding to particle B in Figure 1). Furthermore, the sharp diffraction spots of the SAED pattern of $Sr_2Si_5N_8$ indicate a better crystallinity of $Sr_2Si_5N_8$ in comparison with Sr_2SiO_4. This will result in an intense luminescence of the Eu^{2+}-activated $Sr_2Si_5N_8$ as shown below. The EDS spectrum of $Sr_2Si_5N_8$ (Figure 3e) also confirms the dissolution of oxygen in $Sr_2Si_5N_8$. The introduction of oxygen into the lattice of $Sr_2Si_5N_8$ will affect its luminescence properties, for example, blue shift of the emission spectrum, as will be discussed in the following section.

Analyzing the above results, we propose that the nitridosilicate $Sr_2Si_5N_8$ and the silicate Sr_2SiO_4 are produced by the following chemical reaction:

$$2Si_3N_4 + 4SrCO_3 \rightarrow Sr_2Si_5N_8 + Sr_2SiO_4 + 4CO_2 \quad (4)$$

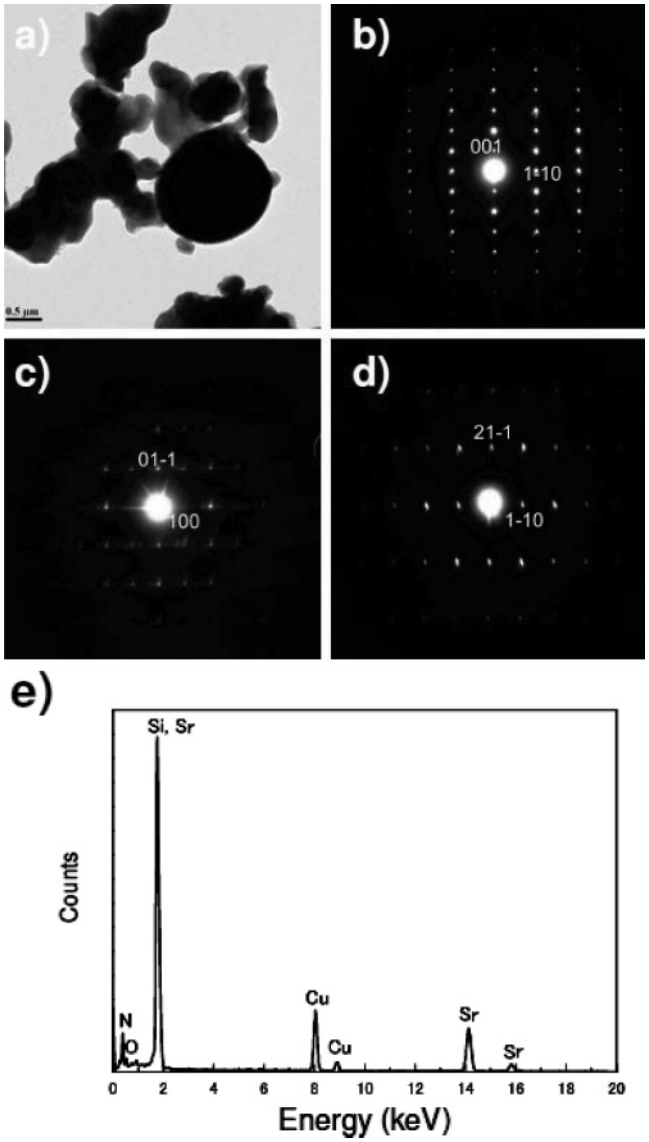

Figure 3. (a) Transmission electron microscopy of the as-synthesized powder by route 3. Selected area diffraction patterns of (b) $Sr_2Si_5N_8$, (c) α-Sr_2SiO_4, and (d) β-Sr_2SiO_4. (e) Energy dispersive spectrum of $Sr_2Si_5N_8$.

The faceted geometry of $Sr_2Si_5N_8$ and the spherical morphology of Sr_2SiO_4 indicate that the above reaction proceeds predominantly through a liquid-assisted solid-state reaction. We then suggest that the reaction progresses through the following sequences: (i) formation of the $SrO-SiO_2$ liquid; (ii) precipitation of Sr_2SiO_4 from the eutectic liquid; (iii) dissolution of Si_3N_4 into the liquid phase; (iv) crystallization of $Sr_2Si_5N_8$ from the nitrogen-saturated liquid. The liquid-assisted reaction process may contribute to fast formation and improved crystallinity of $Sr_2Si_5N_8$ particles, with respect to those methods (routes 1 and 2) entirely based on solid-state reactions which require a relatively long period to complete the reaction and to obtain well-crystallized particles. Calculated from (4), the ideal weight percentage of products $Sr_2Si_5N_8$ and Sr_2SiO_4 is 61.5 and 38.5%, respectively. The quantitative analysis is very close to that estimated from the refinement results. As discussed below, Sr_2SiO_4 has no

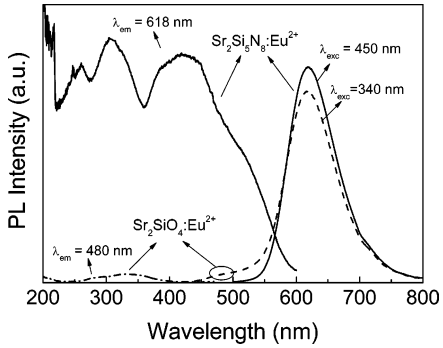

Figure 4. Photoluminescence spectra of the as-synthesized $(Sr_{1.98}Eu_{0.02})Si_5N_8$:$Eu^{2+}$ powder by route 4.

significant impacts on the luminescence properties of $Sr_2Si_5N_8$:Eu^{2+}, which enables the complex phosphor to behave like a single $Sr_2Si_5N_8$:Eu^{2+}.

The phosphor with a nominal composition of $(Sr_{1.98}Eu_{0.02})Si_5N_8$ was synthesized by firing the appropriate amounts of Si_3N_4, $SrCO_3$, and Eu_2O_3 at 1600 °C for 2 h under 0.5 MPa N_2. Figure 4 presents the photoluminescence spectra of the phosphor powder after firing. The excitation spectrum of the complex phosphor consisting of $Sr_2Si_5N_8$:Eu^{2+} and Sr_2SiO_4:Eu^{2+} is similar to that of $Sr_2Si_5N_8$:Eu^{2+} reported in the literature,[11,16,18] showing a broad band covering the spectral range of 200−600 nm when it is monitored at $\lambda_{em} = 618$ nm. The complex phosphor has high absorption and highly efficient excitation in the spectral range of 400−480 nm, perfectly matching with the radiative blue light from InGaN-based LEDs. The emission of the complex phosphor reveals a single and symmetric broad band centered at $\lambda = 618$ nm with a full width of half emission maximum of 83 nm under 450 nm excitation, which is also identical with that of $Sr_2Si_5N_8$:Eu^{2+}.[11,16,18] An additional emission shoulder is observed in the range of 450−560 nm when excited at $\lambda_{exc} = 340$ nm. Blasse et al.[23] has reported that the emission of Sr_2SiO_4:Eu^{2+} exhibits two broad bands centered at 470 and 560 nm under the 254 nm excitation, respectively. Therefore, the emission shoulder is attributable to the emission of Sr_2SiO_4:Eu^{2+} rather than $Sr_2Si_5N_8$:Eu^{2+}. Obviously, Sr_2SiO_4:Eu^{2+} has significantly lower emission levels (i.e., only 0.04% of the intensity of $Sr_2Si_5N_8$:Eu^{2+}) than $Sr_2Si_5N_8$:Eu^{2+} in the complex phosphor, perhaps owing to its lower crystallinity and its emission reabsorbed by $Sr_2Si_5N_8$:Eu^{2+} (the excitation spectrum of $Sr_2Si_5N_8$:Eu^{2+} covers the emission spectrum of Sr_2SiO_4:Eu^{2+}). In addition, Sr_2SiO_4:Eu^{2+} does not absorb blue lights ($\lambda = 400-480$ nm), and its emission is silent under the blue light irradiation. Therefore, it can be concluded that the complex phosphor resembles a single $Sr_2Si_5N_8$:Eu^{2+}, and its luminescence solely comes from $Sr_2Si_5N_8$:Eu^{2+}, upon excitation by blue lights.

Figure 5a shows the emission intensity and the peak emission wavelength of $(Sr_{2-x}Eu_x)Si_5N_8$ prepared by route 4 as a function of Eu concentration. The optimal emission intensity is observed for the material doped with 2 atom % Eu (i.e., $x = 0.4$), which is consistent with that prepared by route 3 (ref 18). The emission intensity declines slowly as

(22) Brindley, G. W. *Philos. Mag.* **1945**, *36*, 347.

(23) Blasse, G.; Bril, A. *Philips Res. Rep.* **1968**, *23*, 201.

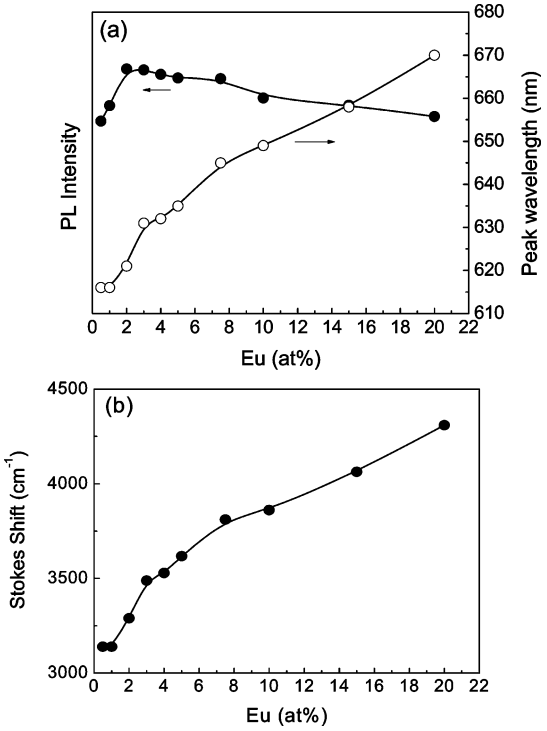

Figure 5. (a) The emission intensity of $(Sr_{2-x}Eu_x)Si_5N_8$ (route 4) as a function of the Eu concentration; (b) the changes in Stokes shift as a function of Eu^{2+} concentration.

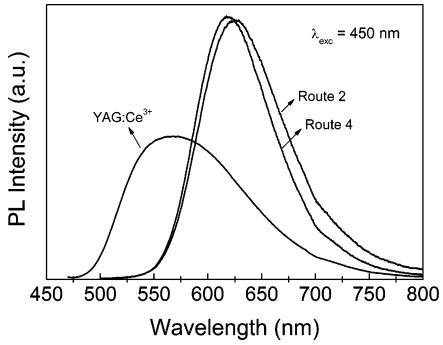

Figure 6. Emission spectra of $(Sr_{1.98}Eu_{0.02})Si_5N_8:Eu^{2+}$ phosphors (λ_{exc} = 450 nm) synthesized by route 2 and route 4, respectively. The emission spectrum of a standard YAG:Ce^{3+} (P46-Y3) is also included for comparison (λ_{exc} = 460 nm).

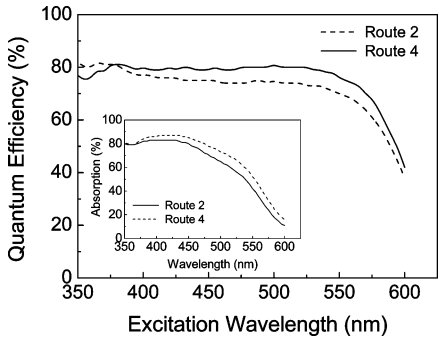

Figure 7. Quantum efficiency and absorption of $(Sr_{1.98}Eu_{0.02})Si_5N_8:Eu^{2+}$ phosphors synthesized by route 2 and route 4, respectively.

the concentration of Eu^{2+} exceeds 2 atom %. Meanwhile, the peak emission of $Sr_2Si_5N_8:Eu^{2+}$ shifts to the long-wavelength side (red shift) with increasing the Eu^{2+} concentration. The red shift in emission spectrum is frequently observed in rare-earth-doped phosphors as the dopant level increases.[3,5,6,9] It is often ascribed to the changes in crystal field strength surrounding the activators[3,5,6,9] because the incorporation of dopants into the lattice would cause the expansion or shrinkage of the unit, the changes in the bond length, covalency, and symmetry, and so on. One of the phenomenological characteristics of the variation of the crystal field strength is the significant changes in the position and shape of the excitation band. However, in our case the excitation spectrum hardly varies except the intensity with changes in the Eu concentration, indicative of no significant changes in crystal field strength. It is possibly due to the fact that (i) Sr^{2+} (1.18 Å, 6CN) and Eu^{2+} (1.17 Å, 6CN) have a similar ionic size;[24] (ii) $Sr_2Si_5N_8$ and $Eu_2Si_5N_8$ are isostructural with orthorhombic crystal system,[17,25] (iii) Sr−N and Eu−N bonds have almost equivalent bond lengths in the range of 2.60−3.25 Å.[17,25] Figure 5b shows the Stokes shift as a function of the Eu^{2+} concentration. It is clearly seen that the Stokes shift increases with increasing the Eu^{2+} concentration. Based on the fact that the crystal field strength does not change greatly, the observed red shift is therefore dominantly attributed to the increased Stokes shift. Of course, the contribution of reabsorption for the observed red shift cannot be ruled out.[3,5,6]

The emission spectra of $(Sr_{1.98}Eu_{0.02})Si_5N_8$ phosphors prepared by route 2 and route 4 and a standard YAG:Ce^{3+} (P46-Y3) are compared in Figure 6. As seen, $Sr_2Si_5N_8:Eu^{2+}$ prepared by route 4 emits strongly at λ_{em} = 616 nm, about 9 nm shorter than that prepared by route 2 (λ_{em} = 625 nm). The blue shift of emission in $Sr_2Si_5N_8:Eu^{2+}$ prepared by route 4 is due to the dissolution of oxygen in the lattice which reduces the covalency and crystal field splitting. Both phosphors have the same emission intensity under the 450 nm excitation, the intensity of which is as high as about 200% of YAG:Ce^{3+}. Besides the emission spectra, both the external and internal quantum efficiencies (QEs) of $Sr_2Si_5N_8:Eu^{2+}$ were also measured and calculated using the method proposed in ref 26. Figure 7 shows the internal quantum efficiency and absorption of $Sr_2Si_5N_8:Eu^{2+}$ prepared by route 2 and route 4, respectively, as a function of excitation wavelength. As seen, the internal quantum efficiency of $Sr_2Si_5N_8:Eu^{2+}$ prepared by route 4 is about 3−6% higher than that prepared by route 2, but its absorption is about 3−8% lower than that of the latter one (see the insert in Figure 7), in the whole excitation wavelength of 400−480 nm. This finally results in equivalent external quantum efficiency for both phosphors when excited at λ = 400−480 nm. For example, the external QE is about 64% for both phosphors at λ_{exc} = 450 nm. It thus implies that the optical properties of the $Sr_2Si_5N_8:Eu^{2+}$-based red phosphor synthesized by route 4 are analogous to those of $Sr_2Si_5N_8:Eu^{2+}$ prepared by route 2 when it is excited by the blue light.

It is generally required that phosphors for white LEDs should have low thermal quenching for avoiding the changes in chromaticity and brightness of white LEDs. The temper-

(24) Shannon, R. D. *Acta Crystallogr., Sect. A* **1976**, *32*, 751.
(25) Huppertz, H.; Schnick, W. *Acta. Crystallogr., Sect. C* **1997**, *53*, 1751.
(26) Ohkubo, K.; Shigeta, T. *J. Illum. Eng. Inst. Jpn.* **1999**, *83*, 87.

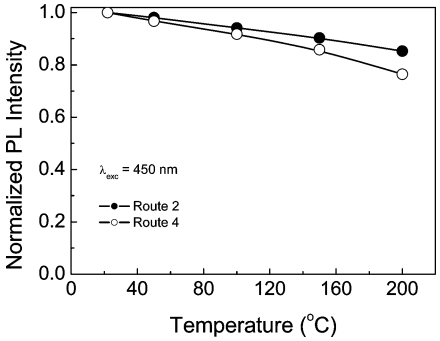

Figure 8. Temperature dependence of PL intensity of $(Sr_{1.98}Eu_{0.02})Si_5N_8$:$Eu^{2+}$ phosphors synthesized by route 2 and route 4, respectively.

ature-dependent emission intensity of $Sr_2Si_5N_8$:Eu^{2+} prepared by route 2 and route 4 was measured at 25−200 °C, as illustrated in Figure 8. At 150 °C, the emission intensity of $Sr_2Si_5N_8$:Eu^{2+} prepared by route 2 and route 4 remains at about 90 and 86% of that measured at 25 °C, indicating that both phosphors show very low thermal quenching. The slightly high thermal quenching of $Sr_2Si_5N_8$:Eu^{2+} prepared by route 4 is due probably to the existing silicate Sr_2SiO_4, which exhibits a high thermal quenching.[23] The thermal quenching of $Sr_2Si_5N_8$:Eu^{2+} prepared by route 4 is smaller than that prepared by the CRN method (route 3) which has only 80% of the initial intensity at 150 °C.[18]

4. Conclusions

We have reported a novel synthetic route to $Sr_2Si_5N_8$:Eu^{2+}-based red phosphors for white light-emitting diodes, through the chemical reaction of $SrCO_3$, Eu_2O_3, and Si_3N_4 at 1600 °C under 0.5 MPa N_2. This method promises the use of inexpensive, commercially available, air-insensitive starting powders and powder handling in an ambient atmosphere, thus offering a simple, efficient, and high-yield way to $Sr_2Si_5N_8$:Eu^{2+}. The synthesized phosphor is a complex mixture consisting of $Sr_2Si_5N_8$:Eu^{2+} (∼64 wt %) and Sr_2SiO_4:Eu^{2+} (∼36 wt %), but the latter does not give emissions under the blue light excitation, making the complex phosphor resemble a single $Sr_2Si_5N_8$:Eu^{2+} phosphor. The $Sr_2Si_5N_8$:Eu^{2+}-based phosphor exhibits equivalent luminescence properties, such as high emission intensity, high conversion efficiency, and very low thermal quenching, to those fabricated by conventional methods. This approach is also applicable to synthesis of $Ca_2Si_5N_8$:Eu^{2+} and $Ba_2Si_5N_8$:Eu^{2+} red phosphors.

Acknowledgment. This work was financially supported by the Grants-in-Aid for Encouragement of Young Scientists (B) with Contract No. 17760550 from the Japan Society for the Promotion of Science (JSPS).

CM061010N